nature geoscience

ARTICLES

https://doi.org/10.1038/s41561-021-00870-6

Earth's missing argon paradox resolved by recycling of oceanic crust

Jonathan M. Tucker[1,2] ✉, Peter E. van Keken[1] and Chris J. Ballentine[3]

The extent to which primordial mantle domains have survived billions of years of convective mixing is a fundamental question in mantle dynamics and geochemistry. The observation that around half of Earth's ^{40}Ar is missing from the atmosphere has been used to argue for a largely primordial, convectively isolated lower mantle. This hypothesis is apparently supported by lower ^{40}Ar/^{36}Ar ratios in the mantle source of ocean-island basalts compared with mid-ocean-ridge basalts. However, strongly layered convection is contradicted by seismic tomographic observations and geodynamic constraints. Using joint geodynamic–geochemical modelling of mantle convection, we show that high ^{40}Ar concentrations associated with K-rich subducted oceanic crust plus unmelted material dispersed throughout the mantle can fully account for Earth's ^{40}Ar budget. This solution to the missing Ar paradox requires neither a substantial reduction in Earth's assumed K concentration nor large isolated domains in the mantle. We additionally show that subducted atmosphere-derived Ar has little effect on the mantle ^{40}Ar budget but can substantially reduce mantle ^{40}Ar/^{36}Ar ratios. Unlike He and Ne isotope systems, whose variations reflect primarily incorporation of primordial material, mantle ^{40}Ar/^{36}Ar ratios may instead result from subduction of atmosphere-derived Ar into the deep mantle.

Terrestrial processes associated with mantle convection and plate tectonics continually modify the chemistry of Earth's mantle, crust and atmosphere. Radiogenic noble gases produced by long-lived radioactive parents are sensitive tracers of the dynamic history of the mantle and of the exchange of volatiles between Earth's interior and exterior. The K–Ar system (^{40}K → ^{40}Ar, half-life 1.25 Gyr) is particularly well suited to study the extent of outgassing and hence mantle processing rate over Earth history. Specifically, the observation that much of Earth's radiogenic ^{40}Ar does not reside in the atmosphere has been interpreted to indicate that massive mantle domains have remained unprocessed by partial melting and degassing[1,2].

Because nearly all terrestrial ^{40}Ar is produced from ^{40}K decay, the fraction of ^{40}Ar accounted for by the atmospheric budget depends only on the assumed bulk silicate Earth (BSE) K concentration. For a BSE K concentration between 190 and 280 ppm, only ~40–60% of Earth's ^{40}Ar is in the atmosphere (Extended Data Figure 1). The continental crust and upper mantle contain at most a few percent of Earth's ^{40}Ar[2]. The substantial portion of Earth's ^{40}Ar not accounted for by the atmosphere, crust and upper mantle has been termed 'missing Ar'[2].

The conventional explanation for the large amount of missing Ar is that it resides in mantle domains that have not been subject to partial melting and degassing[1,2]. This simple explanation has been used as evidence for convective isolation of the upper and lower mantle, with the lower mantle remaining largely primordial. ^{40}Ar/^{36}Ar ratios in mid-ocean-ridge basalts (MORBs) and ocean-island basalts (OIBs) appear to support this explanation: MORBs tend to have higher ^{40}Ar/^{36}Ar ratios than OIBs[3], which by analogy to ^{4}He/^{3}He and ^{21}Ne/^{22}Ne could reflect a higher degree of processing and outgassing of the MORB mantle compared with the OIB mantle. However, strongly layered convection is inconsistent with seismological observations of material exchange between the upper and lower mantle via slabs[4] and plumes[5], as well as geodynamic evidence[6–8], which presents a paradox.

Previously proposed resolutions to this missing Ar paradox fall into two classes: either material exchange between the upper and lower mantle is relatively limited[9,10] or the BSE K concentration has been overestimated[11–13]. In this article, we demonstrate the plausibility of the hypothesis that ^{40}Ar produced from ^{40}K decay within ancient oceanic crust sequestered in the deep mantle alleviates the need for either an isolated primordial reservoir or reduction of the BSE K concentration. We also demonstrate that recycling of atmosphere-derived Ar into the mantle, rather than preservation of undegassed domains, may be a critical factor controlling mantle ^{36}Ar concentrations and ^{40}Ar/^{36}Ar variability.

Models of K–Ar in whole-mantle convection

We utilize models of thermochemical mantle convection in a cylindrical geometry[14] with tracers tracking ^{40}K, ^{40}Ar and ^{36}Ar compositions (Fig. 1 and Methods). Because the K–Ar system speaks directly to the time-integrated mantle processing history over 4.55 Gyr, the models used match Earth's convective vigour expressed as plate speeds, surface heat flow and melting rates. It is crucial to include the effect of oceanic crust subduction on the K–Ar system as K is strongly concentrated into the oceanic crust during partial melting. We assume five different values for the relative density excess of oceanic crust to average mantle $d\ln\rho$ ($= d\rho/\rho$)—2.6%, 3.8%, 4.5%, 5.1% and 6.4%—and refer to these as models $d\ln\rho26$, $d\ln\rho38$, $d\ln\rho45$, $d\ln\rho51$ and $d\ln\rho64$[15]. These five models simulate 4.55 Gyr of solid mantle convection with similar and Earth-like convective vigour. In a sixth model, $d\ln\rho64ts$, we rescale the $d\ln\rho64$ model time to simulate enhanced early convective vigour (Methods).

An important feature of our modelling set-up is that the geochemical modelling is performed as an efficient post-processing step independent of the computationally much more expensive geodynamic modelling. This allows us to explore wide ranges of geochemical parameters rather than assuming values a priori. We use a Markov chain Monte Carlo (MCMC) procedure to constrain six geochemical parameters, resulting in models optimally matching

[1]Earth and Planets Laboratory, Carnegie Institution for Science, Washington DC, USA. [2]Department of Mineral Sciences, National Museum of Natural History, Smithsonian Institution, Washington DC, USA. [3]Department of Earth Sciences, University of Oxford, Oxford, UK. ✉e-mail: tuckerjm@si.edu

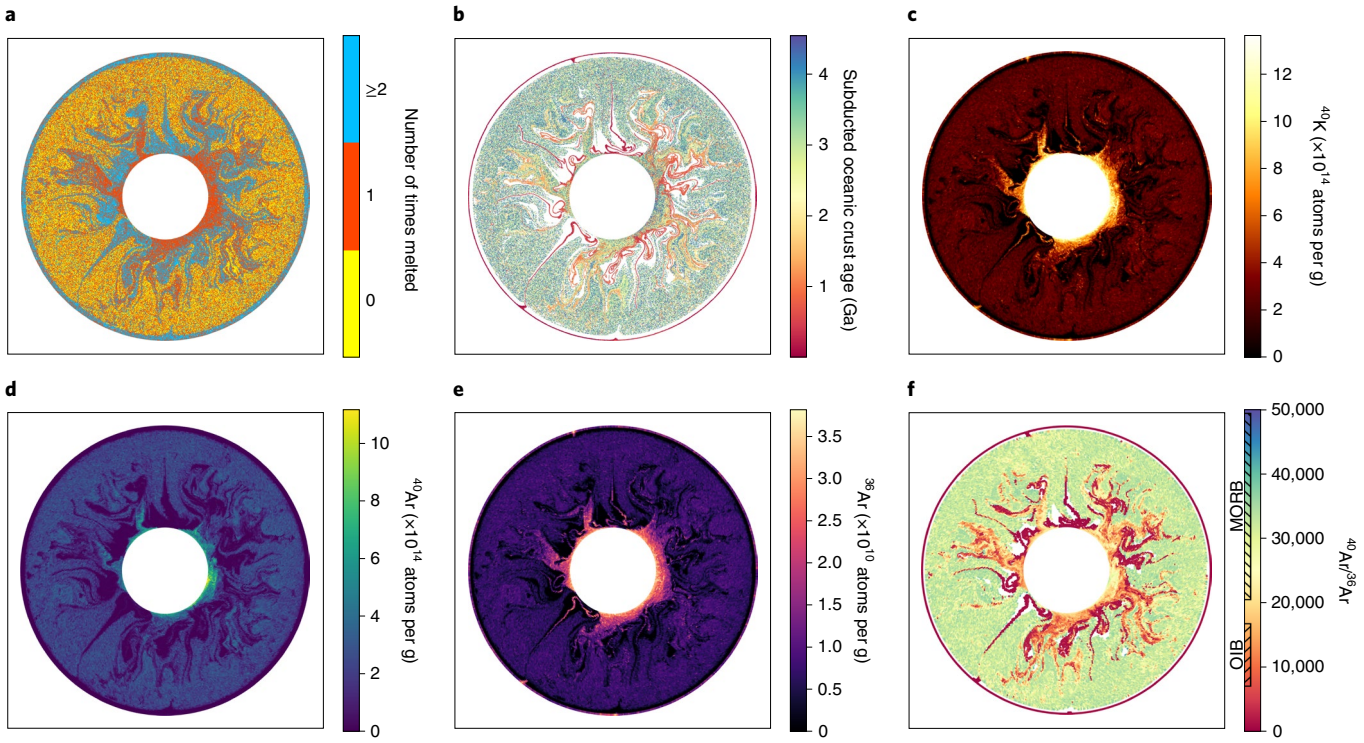

Fig. 1 | Tracer distribution and compositions in the final model time step (4.55 Gyr). Results here are for the dlnρ64 model; other models are shown in Supplementary Figs. 13–16. **a**, Distribution of unmelted (yellow) and melted (red, blue) tracers. The lowermost mantle is dominated by processed (melted) material whereas primordial (unmelted) material is distributed throughout the mantle. **b**, Age (time since last melting) of oceanic crust (eclogite tracers). Young crust traverses the mantle quickly and accumulates near the core–mantle boundary. **c**, Distribution of ^{40}K. Subducting oceanic crust delivers ^{40}K to the lower mantle where it eventually decays to ^{40}Ar. **d**, Distribution of ^{40}Ar. ^{40}Ar is absent from young subducted crust but is present in areas of primordial mantle and ancient oceanic crust. ^{40}Ar derived from subducted ^{40}K in ancient oceanic crust alleviates the need for all the mantle's missing Ar to reside in primordial domains. **e**, Distribution of ^{36}Ar. In addition to primordial domains, high ^{36}Ar concentrations are associated with subducted oceanic crust due to atmosphere-derived Ar incorporated into the subducting crust. **f**, Distribution of ^{40}Ar/^{36}Ar ratios. ^{40}Ar/^{36}Ar variations largely reflect variations in subducted atmosphere-derived Ar, suggesting atmosphere-derived Ar exerts a strong control on mantle ^{40}Ar/^{36}Ar ratios. Measured MORB and OIB ranges[3] are indicated on the colour bar. Several hundred proximal tracer compositions are averaged to aid visualization in **c**–**f**.

the major observations of the K–Ar system (Methods and Supplementary Figs. 1–12). These parameters are the initial distribution of ^{36}Ar between the mantle and atmosphere (fraction of ^{36}Ar initially in the mantle, ϕ_{Ar}^{mantle}); the Archaean (0–2 Gyr, E_K^1) and post-Archaean (2.00–4.55 Gyr, E_K^2) efficiency of K extraction from subducting oceanic crust to the continental crust (where 0 Gyr is the model start and 4.55 Gyr is the present day); the efficiency of K and Ar recycling from the continental crust and atmosphere to the mantle (R_K and R_{Ar}); and the BSE K concentration (K_{BSE}). Models employing optimized parameter values (listed in Table 1) are summarized in Supplementary Tables 1–6 and are the basis for our analysis.

Missing Ar in ancient oceanic crust

The crux of the missing Ar paradox is the presumption that radiogenic ^{40}Ar in the mantle resides in primordial domains that have not lost their Ar to the atmosphere, requiring a large amount of preserved primordial mantle[2]. However, our models explore the previously overlooked possibility that some mantle ^{40}Ar may instead be associated with ancient oceanic crust rather than primordial material. Ancient oceanic crust has long been recognized as crucial to mantle geodynamics and geochemistry[16–18].

Accumulation of radiogenic ^{40}Ar in ancient oceanic crust occurs as long as some K is retained in subducting oceanic crust. Although highly incompatible elements such as K are strongly concentrated in the continental crust, they may also be abundant in ancient oceanic crust[19]. During mid-ocean-ridge melting, K is efficiently transferred from residual mantle lithosphere to the oceanic crust. K is further enriched in the upper crust during low-temperature seafloor alteration[20]. Some K loss from dykes and gabbros may occur during high-temperature alteration, although much of the original K is likely to remain[20]. While K in the upper crust may be released to the mantle wedge through dehydration or melting during subduction, the lower crust is less susceptible to these effects[21]. Therefore, retention of some K in oceanic crust through subduction is expected.

In our models, K is retained in subducting oceanic crust as long as the extraction efficiency parameters are less than 1. In the MCMC trials, post-Archaean K extraction parameters (E_K^2) are generally greater than 0.5 (Table 1), commensurate with its high incompatibility and fluid mobility. Archaean K extraction parameters (E_K^1) vary from 0 to 1 and strongly negatively correlate with the BSE K concentrations (Supplementary Figs. 7–12). This negative correlation probably reflects the use of the continental crust K concentration as a constraint—if the BSE K concentration were increased, the extraction efficiency must decrease to match the continental crust K content. However, the probability of E_K^1 and E_K^2 being simultaneously close to 1 is very low (Supplementary Figs. 7–12).

An increase in K extraction efficiency from the Archaean to post-Archaean ($E_K^2 > E_K^1$) may appear to contradict other models based on the K–Ar system where continental crust grew rapidly in the Archaean to near its present mass[22,23]. However, we note that

Table 1 | Parameters optimized by MCMC sampling

Parameter	Prior distribution	Posterior distribution (median and middle 95%)					
		dlnρ26	dlnρ38	dlnρ45	dlnρ51	dlnρ64	dlnρ64ts
ϕ_{Ar}^{mantle}	0–1	$0.014^{+0.027}_{-0.013}$	$0.015^{+0.03}_{-0.014}$	$0.016^{+0.03}_{-0.015}$	$0.016^{+0.03}_{-0.015}$	$0.014^{+0.035}_{-0.014}$	$0.018^{+0.041}_{-0.017}$
E^1_K	0–1	$0.45^{+0.47}_{-0.43}$	$0.44^{+0.51}_{-0.42}$	$0.43^{+0.52}_{-0.42}$	$0.42^{+0.55}_{-0.4}$	$0.39^{+0.56}_{-0.38}$	$0.46^{+0.5}_{-0.42}$
E^2_K	0–1	$0.76^{+0.23}_{-0.54}$	$0.75^{+0.23}_{-0.56}$	$0.77^{+0.22}_{-0.6}$	$0.82^{+0.17}_{-0.57}$	$0.79^{+0.2}_{-0.6}$	$0.76^{+0.23}_{-0.68}$
R_K	0–10	$2.5^{+5.3}_{-2.4}$	$2.5^{+5.4}_{-2.4}$	$2.5^{+5.6}_{-2.3}$	$3.7^{+5.2}_{-3.5}$	$3.2^{+5.8}_{-3.1}$	$3.5^{+5.9}_{-3.3}$
R_{Ar}	0–2	$0.011^{+0.022}_{-0.01}$	$0.013^{+0.025}_{-0.012}$	$0.015^{+0.031}_{-0.014}$	$0.019^{+0.043}_{-0.018}$	$0.03^{+0.052}_{-0.028}$	$0.03^{+0.06}_{-0.028}$
K_{BSE} (ppm)	150–300	160^{+10}_{-9}	168^{+13}_{-14}	176^{+16}_{-18}	188^{+18}_{-22}	206^{+26}_{-30}	221^{+48}_{-41}

Prior distributions are the uniform ranges from which MCMC samples are drawn. The median and middle 95% of the posterior distributions are considered the 'best-fit' values and a measure of their uncertainties.

those models also merely consider the extraction of K to the continental crust. Therefore, inefficient Archaean K extraction does not obviate early continental crust growth; it could instead indicate that early continental crust was relatively K poor, consistent with observations that the continental crust became more felsic over time[24,25].

Some K may also be eroded from the continents and recycled with subducting slabs[26]. The correlation between the extent of continental crustal K recycling (R_K) and the post-Archaean K extraction efficiency (E^2_K) (Supplementary Figs. 7–12) also likely results from use of the continental crust K concentration as a model constraint. The lack of correlation between R_K and E^1_K may be because the K content of the continental crust remains low early in the models.

Any ^{40}K remaining in oceanic crust through subduction eventually decays to ^{40}Ar, creating a reservoir of mantle ^{40}Ar independent of primordial material. This reservoir is substantial in our best-fit models—almost 40% of the mantle ^{40}Ar resides in ancient oceanic crust rather than unmelted mantle (Supplementary Tables 1–6). Consequently, the fraction of primordial (unmelted) mantle is substantially lower than the fraction of missing Ar (Fig. 2a,b; see also ref. [27]). For example, in the dlnρ64 model, almost half of Earth's ^{40}Ar is in the mantle, yet only a quarter of the mantle mass is unmelted (Supplementary Table 5). Our models therefore demonstrate that production and storage of ^{40}Ar from ^{40}K in ancient oceanic crust alleviates the requirement for all mantle ^{40}Ar to reside in large isolated primordial domains, providing a simple resolution to the missing Ar paradox.

Unmelted material in our models is not concentrated in the lower mantle, but rather distributed throughout the mantle (Fig. 1a). This is because slabs quickly penetrate vertically to the lower mantle, displacing older material upwards[14] (Methods). While this whole-mantle convection endmember behaviour may not be entirely realistic and could have other unintended geochemical consequences[19], it raises the possibility that that proposed high-density and primordial lower mantle domains[28–30] may not be needed.

Is Earth's K concentration overestimated?

The BSE K concentration directly determines Earth's ^{40}Ar content and consequently the amount of missing ^{40}Ar. Estimates of the BSE K concentration, generally inferred from the BSE U concentration and K/U ratio, range from 190 to 280 ppm (Extended Data Fig. 1). The BSE K/U ratio is often thought to be less certain than the U concentration, and downward revision could reduce the magnitude of the missing Ar paradox[11–13]. The BSE K/U ratio is typically inferred from MORBs[31,32], requiring the assumption that K and U do not fractionate during tectonic processes. Lassiter[13] argued that dehydration during subduction causes subducted oceanic crust to carry particularly low K/U ratio and that the BSE K/U ratio is lower than that estimated from MORBs alone. However, we argue that K/U fractionation during subduction is unlikely to strongly affect the global K and U budgets because the continental crust does not have a complementary high K/U ratio, but rather a ratio similar to the MORB average (Extended Data Fig. 2). We therefore argue that there is no strong evidence for a BSE K/U ratio substantially lower than the MORB value.

Our MCMC procedure allows us to examine the conditions under which different values of K_{BSE} can be accommodated rather than assuming any particular value. We find that although lower values (160–200 ppm K) are more probable, higher values are permissible in models with high oceanic crust density (dlnρ) and low initial continental crust extraction efficiency (E^1_K) (Table 1 and Supplementary Fig. 11). Such parameter values restrict K from entering the continental crust such that the crust and atmosphere do not accumulate too much ^{40}K and ^{40}Ar, respectively. These parameter values are also geologically plausible as ample geophysical and geochemical evidence supports dense oceanic crust accumulation in the lower mantle[16–18], and inefficient Archaean K extraction to the continental crust is consistent with the geologic record[24,25].

We therefore conclude that the missing Ar paradox can be reconciled without a convectively isolated lower mantle and without a particularly low BSE K concentration as long as subducted oceanic crust is dense enough to sequester K (and ^{40}Ar) from the rest of the silicate Earth.

Ar subduction explains mantle ^{40}Ar/^{36}Ar variability

The ^{40}Ar/^{36}Ar ratios in the mantle vary by more than any isotope system except ^{4}He/^{3}He, but the origin of this extreme variation is not settled. By analogy to ^{4}He/^{3}He, less-degassed portions of the mantle would have lower ^{40}Ar/^{36}Ar[11,33,34]. Indeed, OIBs have ^{40}Ar/^{36}Ar around 10,000–20,000 whereas MORBs have ^{40}Ar/^{36}Ar between 20,000 and 50,000[3]. However, a global correlation between He and Ar isotopes is quite weak[3]. Alternatively, low ^{40}Ar/^{36}Ar ratios, as well as low ^{129}Xe/^{130}Xe ratios, could be due to preferential addition of atmosphere-derived Ar (^{40}Ar/^{36}Ar = 298.6) to the mantle[35–38], perhaps facilitated by incorporation into hydrous minerals during oceanic crust alteration[39,40]. While the idea of noble gas subduction to the deep mantle had long been opposed[41,42], substantial recent work has demonstrated that noble gases can pass through the 'subduction barrier'[3,35,36,43]. In addition to exploring whether low ^{40}Ar/^{36}Ar ratios are due to primordial material or subducted atmosphere, we investigate whether atmospheric Ar subduction is another possible solution to the missing Ar paradox. Substantial atmosphere-derived ^{40}Ar subducted to the deep mantle could alleviate the need for mantle ^{40}Ar to reside in primordial domains.

Our models permit but do not require subduction of atmosphere-derived Ar as the Ar recycling efficiency parameter (R_{Ar}) can be 0. We find that in the most probable solutions, R_{Ar} is

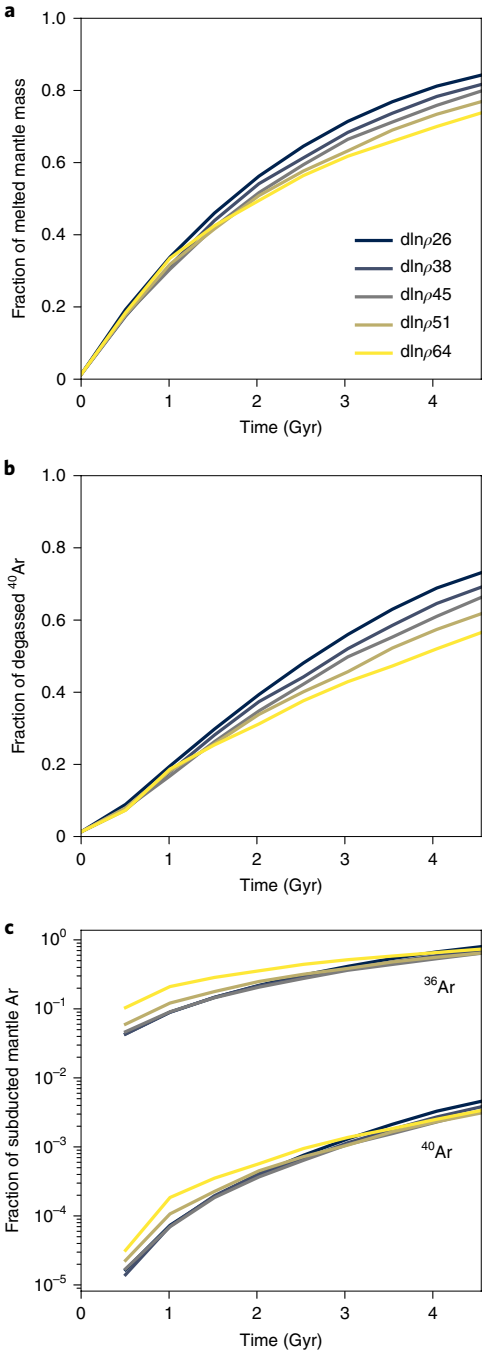

Fig. 2 | Fraction of melted mantle mass, degassed ^{40}Ar and subducted mantle Ar in the five best-fit models. a, By 4.55 Gyr, 74–84% of the mantle mass has been melted at least once, meaning only 16–26% remains primordial. **b**, The fraction of degassed ^{40}Ar is lower than the fraction of unmelted mantle due to ^{40}Ar storage in subducted oceanic crust. This negates the requirement for large volumes of primordial material to account for Earth's missing Ar. **c**, The fraction of mantle ^{36}Ar subducted from the atmosphere is substantial (64–80% by 4.55 Gyr), but the fraction of ^{40}Ar is negligible (<1%). Due to their relative ^{40}Ar/^{36}Ar ratios, subduction much more strongly affects mantle ^{36}Ar than ^{40}Ar.

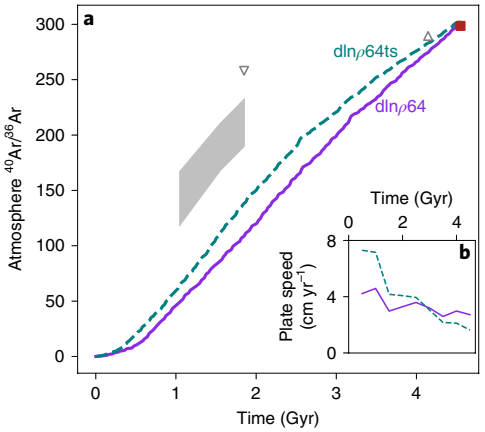

Fig. 3 | Comparison of models with constant convective vigour and enhanced early convective vigour. a, Both the constant convective vigour model (dlnρ64) and the enhanced early convective vigour model (dlnρ64ts) match the modern atmospheric composition (red square), but ^{40}Ar/^{36}Ar rises faster in the dlnρ64ts model, approaching the ancient atmosphere measurements (grey box[22], downward triangle[51], upward triangle[52]). **b**, Average plate speeds (500 Myr averages), a proxy for convective vigour, are nearly constant with time in the dlnρ64 model but decrease by a factor of 4 in the dlnρ64ts model.

greater than 0 (Table 1) and much of the ^{36}Ar ultimately residing in the mantle has been subducted from the atmosphere, yet subducted atmosphere-derived ^{40}Ar is almost negligible (Fig. 2c). Because the atmospheric ^{40}Ar/^{36}Ar ratio is much lower than that of the mantle, subduction of atmosphere-derived Ar affects ^{36}Ar substantially more than ^{40}Ar. High ^{36}Ar concentrations near the core–mantle boundary are due to subduction of atmosphere-derived Ar, whereas coincident high ^{40}Ar concentrations are due to ^{40}K decay within ancient oceanic crust (Fig. 1d).

The spatial distribution of ^{40}Ar/^{36}Ar ratios strongly mirrors that of ^{36}Ar (Fig. 1f), demonstrating that ^{40}Ar/^{36}Ar ratios are also modulated by subducted atmosphere-derived Ar. Whereas He and Ne isotopic ratios primarily reflect a mantle domain's outgassing history, our results support the hypothesis that Ar, Kr and Xe isotope ratios, such as the low ^{40}Ar/^{36}Ar and ^{129}Xe/^{130}Xe ratios in OIBs and some MORBs, are strongly influenced by subducted atmosphere-derived noble gases[35–38]. Although subducting plates carrying atmosphere-derived Ar should also have extremely high (U + Th)/^{3}He and consequently elevated ^{4}He/^{3}He ratios, their He concentration is probably too low to overprint low ^{4}He/^{3}He in OIBs associated with primordial material (Methods). Therefore, mantle isotopic ratios of He (and Ne) may be effectively decoupled from Ar (and Kr, Xe) as the former are more sensitive to primordial material and the latter are more dependent on subducted atmosphere-derived noble gases.

The amount of atmosphere-derived Ar subduction in our models depends strongly on the initial ^{36}Ar distribution between the mantle and atmosphere ($\phi_{\mathrm{Ar}}^{\mathrm{mantle}}$), evidenced by the negative correlations between R_{Ar} and $\phi_{\mathrm{Ar}}^{\mathrm{mantle}}$ in the MCMC trials (Supplementary Figs. 7–12). With less ^{36}Ar starting in the mantle, more atmospheric Ar subduction is required, and vice versa. But even when Ar subduction is minimal, more than 90% of the ^{36}Ar is in the atmosphere at the start of our models ($\phi_{\mathrm{Ar}}^{\mathrm{mantle}} < 0.1$).

Our models do not explicitly consider previous events such as late accretion or giant impact-induced catastrophic outgassing. Early outgassing appears to be required by He–Ne[44,45], Ar[22,46] and Xe[47,48] systematics, and late accretion of Earth's volatiles has also been advocated[49,50]. Both of these processes are adequately simulated by low $\phi_{\mathrm{Ar}}^{\mathrm{mantle}}$ values because insignificant ^{40}Ar is produced during Earth's accretionary epoch.

Atmospheric ^{40}Ar/^{36}Ar evolution

While our models are constrained by observations of K and Ar in modern Earth reservoirs, they can also provide predictions for

the time evolution of those reservoirs such as the atmospheric $^{40}Ar/^{36}Ar$ ratio. Data from ancient samples[22,51,52] appear to require higher atmospheric $^{40}Ar/^{36}Ar$ ratios in the past than predicted by our models (Fig. 3), whereas models with faster convective vigour early in Earth history tend to match these observations better[22,23,46]. Furthermore, faster early convective vigour may be required to explain Pu–U–Xe systematics[53,54].

We explore the potential effects of enhanced early convective vigour by rescaling time in our dlnρ64 model (dlnρ64ts; Methods). Rescaling results in approximately twice faster Hadean–Archaean plate speeds compared with the unscaled model (Fig. 3b). We repeat the MCMC procedure using identical constraints to the unscaled models; that is, atmospheric $^{40}Ar/^{36}Ar$ ratio is not forced to higher values early in the model. The best-fit chemical parameters fit the modern K and Ar data equally well as the unscaled models (Supplementary Fig. 6), and the atmospheric $^{40}Ar/^{36}Ar$ ratio does indeed increase earlier than in the unscaled models (Fig. 3a). The dlnρ64ts model does not quite reach the data due to limitations in the timescaling methodology (Methods), but it demonstrates the plausibility of enhanced early convective vigour explaining the data within the context of a fully dynamic model. It also provides an impetus to develop higher-convective-vigour geodynamic models without timescaling, a current challenge in geodynamic modelling[55].

Online content

Any methods, additional references, Nature Research reporting summaries, source data, extended data, supplementary information, acknowledgements, peer review information; details of author contributions and competing interests; and statements of data and code availability are available at https://doi.org/10.1038/s41561-021-00870-6.

Received: 17 February 2021; Accepted: 9 November 2021;
Published online: 13 January 2022

References

1. Turcotte, D. L. & Schubert, G. Tectonic implications of radiogenic noble gases in planetary atmospheres. *Icarus* **74**, 36–46 (1988).
2. Allègre, C. J., Hofmann, A. & O'Nions, K. The argon constraints on mantle structure. *Geophys. Res. Lett.* **23**, 3555–3557 (1996).
3. Parai, R., Mukhopadhyay, S., Tucker, J. M. & Pető, M. K. The emerging portrait of an ancient, heterogeneous and continuously evolving mantle plume source. *Lithos* **346**, 105153 (2019).
4. Kárason, H. & van der Hilst, R. D. Constraints on mantle convection from seismic tomography. *Geophys. Monogr.* **121**, 277–288 (2000).
5. French, S. W. & Romanowicz, B. Broad plumes rooted at the base of the Earth's mantle beneath major hotspots. *Nature* **525**, 95–99 (2015).
6. Spohn, T. & Schubert, G. Modes of mantle convection and the removal of heat from the Earth's interior. *J. Geophys. Res. Solid Earth* **87**, 4682–4696 (1982).
7. Davies, G. F. Geophysical and isotopic constraints on mantle convection: an interim synthesis. *J. Geophys. Res. Solid Earth* **89**, 6017–6040 (1984).
8. McNamara, A. K. & van Keken, P. E. Cooling of the Earth: a parameterized convection study of whole versus layered models. *Geochem. Geophys. Geosyst.* **1**, 2000GC000045 (2000).
9. Xie, S. & Tackley, P. J. Evolution of helium and argon isotopes in a convecting mantle. *Phys. Earth Planet. Inter.* **146**, 417–439 (2004).
10. Gonnermann, H. M. & Mukhopadhyay, S. Preserving noble gases in a convecting mantle. *Nature* **459**, 560–563 (2009).
11. Albarède, F. Time-dependent models of U–Th–He and K–Ar evolution and the layering of mantle convection. *Chem. Geol.* **145**, 413–429 (1998).
12. Davies, G. F. Geophysically constrained mantle mass flows and the ^{40}Ar budget: a degassed lower mantle? *Earth Planet. Sci. Lett.* **166**, 149–162 (1999).
13. Lassiter, J. C. Role of recycled oceanic crust in the potassium and argon budget of the Earth: toward a resolution of the 'missing argon' problem. *Geochem. Geophys. Geosyst.* **5**, Q11012 (2004).
14. Brandenburg, J. P., Hauri, E. H., van Keken, P. E. & Ballentine, C. J. A multiple-system study of the geochemical evolution of the mantle with force-balanced plates and thermochemical effects. *Earth Planet. Sci. Lett.* **276**, 1–13 (2008).
15. Jones, T. D., Maguire, R. R., van Keken, P. E., Ritsema, J. & Koelemeijer, P. Subducted oceanic crust as the origin of seismically slow lower-mantle structures. *Prog. Earth Planet. Sci.* **7**, 17 (2020).
16. Ringwood, A. E. Phase transformations and differentiation in subducted lithosphere: Implications for mantle dynamics, basalt petrogenesis, and crustal evolution. *J. Geol.* **90**, 611–643 (1982).
17. Hofmann, A. W. & White, W. M. Mantle plumes from ancient oceanic crust. *Earth Planet. Sci. Lett.* **57**, 421–436 (1982).
18. Zindler, A. & Hart, S. Chemical geodynamics. *Annu. Rev. Earth Planet. Sci.* **14**, 493–571 (1986).
19. Tucker, J. M., van Keken, P. E., Jones, R. E. & Ballentine, C. J. A role for subducted oceanic crust in generating the depleted mid-ocean ridge basalt mantle. *Geochem. Geophys. Geosyst.* **21**, e2020GC009148 (2020).
20. Jarrard, R. D. Subduction fluxes of water, carbon dioxide, chlorine, and potassium. *Geochem. Geophys. Geosyst.* **4**, 8905 (2003).
21. Syracuse, E. M., van Keken, P. E. & Abers, G. A. The global range of subduction zone thermal models. *Phys. Earth Planet. Int.* **183**, 73–90 (2010).
22. Pujol, M., Marty, B., Burgess, R., Turner, G. & Philippot, P. Argon isotopic composition of Archaean atmosphere probes early Earth geodynamics. *Nature* **498**, 87–90 (2013).
23. Guo, M. & Korenaga, J. Argon constraints on the early growth of felsic continental crust. *Sci. Adv.* **6**, eaaz6234 (2020).
24. Dhuime, B., Wuestefeld, A. & Hawkesworth, C. J. Emergence of modern continental crust about 3 billion years ago. *Nat. Geosci.* **8**, 552–555 (2015).
25. Tang, M., Chen, K. & Rudnick, R. L. Archean upper crust transition from mafic to felsic marks the onset of plate tectonics. *Science* **351**, 372–375 (2016).
26. Coltice, N., Albarède, F. & Gillet, F. ^{40}K–^{40}Ar constraints on recycling continental crust into the mantle. *Science* **288**, 845–847 (2000).
27. van Keken, P. E., Ballentine, C. J. & Porcelli, D. A dynamical investigation of the heat and helium imbalance. *Earth Planet. Sci. Lett.* **188**, 421–434 (2001).
28. Tolstikhin, I. & Hofmann, A. W. Early crust on top of the Earth's core. *Phys. Earth Planet. Int.* **148**, 109–130 (2005).
29. Labrosse, S., Hernlund, J. W. & Coltice, N. A crystallizing dense magma ocean at the base of the Earth's mantle. *Nature* **450**, 866–869 (2007).
30. Ballmer, M. D., Houser, C., Hernlund, J. W., Wentzcovitch, R. M. & Hirose, K. Persistence of strong silica-enriched domains in the Earth's lower mantle. *Nat. Geosci.* **10**, 236–240 (2017).
31. Jochum, K. P., Hofmann, A. W., Ito, E., Seufert, H. M. & White, W. M. K. U and Th in mid-ocean ridge basalt glasses and heat production, K/U and K/Rb in the mantle. *Nature* **306**, 431–436 (1983).
32. Gale, A., Dalton, C. A., Langmuir, C. H., Su, Y. & Schilling, J. G. The mean composition of ocean ridge basalts. *Geochem. Geophys. Geosyst.* **14**, 489–518 (2013).
33. Allègre, C. J., Staudacher, T. & Sarda, P. Rare gas systematics: formation of the atmosphere, evolution and structure of the Earth's mantle. *Earth Planet. Sci. Lett.* **81**, 127–150 (1987).
34. Porcelli, D. & Wasserburg, G. J. Mass transfer of helium, neon, argon, and xenon through a steady-state upper mantle. *Geochim. Cosmochim. Acta* **59**, 4921–4937 (1995).
35. Sarda, P., Moreira, M. & Staudacher, T. Argon–lead isotopic correlation in Mid-Atlantic Ridge basalts. *Science* **283**, 666–668 (1999).
36. Holland, G. & Ballentine, C. J. Seawater subduction controls the heavy noble gas composition of the mantle. *Nature* **441**, 186–191 (2006).
37. Parai, R., Mukhopadhyay, S. & Standish, J. J. Heterogeneous upper mantle Ne, Ar and Xe isotopic compositions and a possible Dupal noble gas signature recorded in basalts from the Southwest Indian Ridge. *Earth Planet. Sci. Lett.* **359**, 227–239 (2012).
38. Tucker, J. M., Mukhopadhyay, S. & Schilling, J. G. The heavy noble gas composition of the depleted MORB mantle (DMM) and its implications for the preservation of heterogeneities in the mantle. *Earth Planet. Sci. Lett.* **355**, 244–254 (2012).
39. Kendrick, M. A., Scambelluri, M., Honda, M. & Phillips, D. High abundances of noble gas and chlorine delivered to the mantle by serpentinite subduction. *Nat. Geosci.* **4**, 807–812 (2011).
40. Jackson, C. R. M., Parman, S. W., Kelley, S. P. & Cooper, R. F. Noble gas transport into the mantle facilitated by high solubility in amphibole. *Nat. Geosci.* **6**, 562–565 (2013).
41. Staudacher, T. & Allègre, C. J. Recycling of oceanic crust and sediments: the noble gas subduction barrier. *Earth Planet. Sci. Lett.* **89**, 173–183 (1988).
42. Burnard, P. G. Origin of argon–lead isotopic correlation in basalts. *Science* **286**, 871 (1999).
43. Matsumoto, T., Chen, Y. & Matsuda, J. Concomitant occurrence of primordial and recycled noble gases in the Earth's mantle. *Earth Planet. Sci. Lett.* **185**, 35–47 (2001).
44. Honda, M. & McDougall, I. Primordial helium and neon in the Earth—a speculation on early degassing. *Geophys. Res. Lett.* **25**, 1951–1954 (1998).
45. Tucker, J. M. & Mukhopadhyay, S. Evidence for multiple magma ocean outgassing and atmospheric loss episodes from mantle noble gases. *Earth Planet. Sci. Lett.* **393**, 254–265 (2014).
46. Sarda, P., Staudacher, T. & Allègre, C. J. $^{40}Ar/^{36}Ar$ in MORB glasses: constraints on atmosphere and mantle evolution. *Earth Planet. Sci. Lett.* **72**, 357–375 (1985).

47. Staudacher, T. & Allègre, C. J. Terrestrial xenology. *Earth Planet. Sci. Lett.* **60**, 389–406 (1982).
48. Porcelli, D., Woolum, D. & Cassen, P. Deep Earth rare gases: initial inventories, capture from the solar nebula, and losses during Moon formation. *Earth Planet. Sci. Lett.* **193**, 237–251 (2001).
49. Drake, M. J. & Righter, K. Determining the composition of the Earth. *Nature* **416**, 39–44 (2002).
50. Hirschmann, M. M. Constraints on the early delivery and fractionation of Earth's major volatiles from C/H, C/N, and C/S ratios. *Am. Mineral.* **101**, 540–553 (2016).
51. Hanes, J. A., York, D. & Hall, C. M. An $^{40}Ar/^{39}Ar$ geochronological and electron microprobe investigation of an Archean pyroxenite and its bearing on ancient atmospheric compositions. *Can. J. Earth Sci.* **22**, 947–958 (1985).
52. Stuart, F. M., Mark, D. F., Gandanger, P. & McConville, P. Earth–atmosphere evolution based on new determination of Devonian atmosphere Ar isotopic composition. *Earth Planet. Sci. Lett.* **446**, 21–26 (2016).
53. Coltice, N., Marty, B. & Yokochi, R. Xenon isotope constraints on the thermal evolution of the early Earth. *Chem. Geol.* **266**, 4–9 (2009).
54. Parai, R. & Mukhopadhyay, S. Xenon isotopic constraints on the history of volatile recycling into the mantle. *Nature* **560**, 223–227 (2018).
55. Jones, T. D., Sime, N. & van Keken, P. E. Burying Earth's primitive mantle in the slab graveyard. *Geochem. Geophys. Geosyst.* **22**, e2020GC009396 (2021).

Methods

Geodynamic modelling. Our models of thermochemical mantle convection are based on those of Brandenburg et al.[14]. Full descriptions of the methodology, equations, initial and boundary conditions, discretization and tests are provided in the original literature[14]. While these models are relatively simple, they are able to explain a number of isotopic patterns seen in MORB and OIB geochemistry[14,56] and therefore provide a useful set of models for further hypothesis testing that relies on the principal mechanism of oceanic crust formation, recycling and storage over the age of Earth. Here we briefly summarize the modelling approach, key features, assumptions and limitations.

The models are based on the solution of the time-dependent heat equation coupled to the Stokes and mass-conservation equations under the assumption of the Boussinesq flow, which implies incompressibility and the absence of solid-state phase transitions. The model geometry is a two-dimensional cylindrical shell with a rescaled core–mantle boundary, which enables Earth-like heat transport properties in mantle convection modelling[57]. The temperature contrast across the mantle is kept constant over geological time. The mantle is assumed to be a Newtonian fluid with three orders of magnitude viscosity variation due to temperature alone with a higher depth-dependent viscosity in the lithosphere and lower mantle. The combined temperature- and depth-dependent effects set up a radially average viscosity profile that is similar to that observed for Earth's mantle (see references in Brandenburg et al.[14]).

Plate-like dynamics are simulated following the approach of Gable et al.[58], which allows for the imposition of kinematic boundary conditions on the Stokes equations that are fully consistent with the dynamics and energetics of the underlying mantle dynamics and allow for models to reach Earth-like convective vigour (see the following). The models' eight fixed plate boundaries are convergent or divergent depending on the plates' relative velocities.

The models contain approximately one million passive 'harzburgite' tracers and an equal number of 'eclogite' tracers with a density excess, all initially evenly spaced throughout the model. Harzburgite tracers contain seven times the volume of eclogite tracers; thus, the initial condition represents a 'lherzolitic' mantle. Following previous work[59], we use these petrological terms that are defined for the uppermost mantle only throughout to refer to the average mantle composition (lherzolite), the oceanic crust (eclogite) and the depleted residue (harzburgite) while recognizing that mineral phase changes would change this terminology with depth. Five models are utilized, where eclogite tracers (with density ρ_E) are assumed to have density excesses over lherzolitic mantle (ρ_L) of $d\ln\rho = (\rho_E - \rho_L)/\rho_L = 2.6\%$, 3.8%, 4.5%, 5.1% and 6.4%.

Oceanic crust formation is simulated by concentrating the eclogite tracers to the top and harzburgite tracers to the bottom of the melting region when tracers enter a divergent plate boundary. This results in oceanic crust and underlying depleted harzburgite layers of similar thicknesses to the averages of present-day Earth. The separation of eclogite and harzburgite tracers during melting influences the model dynamics due to the density contrast of the eclogite and harzburgite layers. Over time, convective mixing causes a marble-cake pattern of intermixed eclogite and harzburgite.

Since the K–Ar system speaks directly to the processing efficiency of the mantle, it is important that the models match Earth-like convective vigour. The original models[14] used an identical Rayleigh number for all eclogite density cases, which resulted in the higher eclogite density models becoming slightly more sluggish over time (see fig. 4 of ref. [14]). Here, we instead adjust the Rayleigh number for each model such that the convective vigour is Earth-like in that the average plate speeds in the last model 500 Ma are approximately 3 cm yr^{-1} on the basis of the poloidal component of the present-day plate tectonic velocity field[60], the surface heat flow is approximately 100 mW m^{-2} (ref. [61]) and the mantle processing rate is approximately 10^{18} g yr^{-1} (ref. [62]).

For an eclogite density higher than that of lherzolite, subducted oceanic crust piles at the base of the mantle (Fig. 1a,b) forming distinct features similar to large low-shear-velocity provinces seen in seismic tomography[15]. Accumulation of subducted oceanic crust in a manner similar to our models occurs ubiquitously in models that use alternative mechanisms for generating plate-like surface behaviour and incorporate compressibility and phase changes[9,63,64]. It also occurs in other model geometries such as rectangles[59,65,66], three-dimensional spheres[63,64] and spherical annuli[55]. Because our models are used primarily to test the hypothesis that subducted oceanic crust is an important reservoir of Earth's ^{40}Ar, the similar dynamic behaviour observed in models using other assumptions suggests that our conclusions do not depend, to first order, on those assumptions.

By contrast, the details of the mantle flow pattern depend on the model set-up. Despite a higher-viscosity lower mantle, downwellings simulating subducting slabs tend to penetrate quickly from convergent boundaries into the lower mantle. This behaviour is not necessarily reflected in Earth's mantle and may affect the distribution of geochemical compositions[19]. We expect that incorporation of mobile plate boundaries, modest mantle compressibility and solid-state phase transitions would slow slab sinking into lower mantle[67], potentially changing the timing and location of accumulated subducted oceanic crust. However, these effects would not necessarily change the conclusion that subducted oceanic crust can host substantial ^{40}Ar, only the spatio-temporal distribution of that crust. A potentially more important change may occur due to Earth's thermal evolution, the strongly correlated changes in melt formation at mid-ocean ridges and the details of when and how plate tectonics began. These processes are difficult to constrain because of limited observations and would introduce new free parameters in the models. We plan to explore the role of compressibility and phase transitions, along with thermal evolution models and associated changes in oceanic crust formation, in future work.

Geochemical modelling. We track the concentrations of ^{40}K, ^{40}Ar and ^{36}Ar in each tracer and track the accumulating number of atoms in the continental crust and atmosphere. Tracer compositions are modified by radioactive decay, partial melting and exchange of elements between the oceanic crust, continental crust and atmosphere. For simplicity, we assume that all chemical differentiation occurs at divergent plate boundaries. K and Ar atoms in melting eclogite and harzburgite tracers are transferred to the eclogite tracers (oceanic crust) on the basis of the assumption that K and Ar are perfectly incompatible ($D=0$). Assuming instead that K and Ar are highly incompatible ($D=0.0001$) and using a batch melting model where the degree of melting is based on the ratio of melting eclogite to harzburgite tracers[14] (a proxy for mantle fertility) has no consequential effect on our results. Some fraction of K in the melting eclogite tracers is extracted to the continental crust controlled by the parameter E_K, and some fraction of continental crust K is recycled back by the parameter R_K[14,56]. Following ref. [14], we allow the value of E_K to change after the Archaean: E^1_K from 0 to 2 Gyr and E^2_K from 2 to 4.55 Gyr. However, we note that this procedure models only K extraction to the continental crust, not the growth of continental crust itself. We assume that Ar is efficiently extracted to the atmosphere and that some atmospheric Ar may be recycled to the melting eclogite tracers by the parameter R_{Ar}. The continental crust accumulates ^{40}Ar from in situ ^{40}K decay, which outgases to the atmosphere after a 500 Myr residence time. This delay simulates ^{40}Ar outgassing associated with crustal reworking and is chosen on the basis that crustal K–Ar ages tend to be a few hundred Myr younger than Rb–Sr ages[68]. The total Earth ^{36}Ar content is set to 3.32×10^{39} atoms on the basis of the present-day atmospheric budget[69,70], considering that the majority of Earth's ^{36}Ar is in the atmosphere[71]. This budget is initially partitioned between the atmosphere and mantle by the parameter ϕ^{mantle}_{Ar}. The Earth is assumed to start with zero ^{40}Ar because nonradiogenic terrestrial ^{40}Ar is negligible[72].

Parameter estimation. Our chemical modelling contains a number of parameters (described in the preceding) that influence the K–Ar evolution. We find values of these parameters that reproduce the major observations from the K–Ar system using MCMC sampling. The main advantage of MCMC sampling over traditional Monte Carlo sampling is that MCMC sampling can estimate the most likely parameter values, their variances and covariances, whereas traditional Monte Carlo sampling can identify only permissible parameter values. In addition, unguided Monte Carlo sampling is much more computationally expensive than MCMC sampling.

Our MCMC sampling finds parameter sets that minimize the misfit between modelled and observed atmospheric ^{40}Ar, continental crust ^{40}K content, atmospheric ^{40}Ar/^{36}Ar ratio and bulk mantle ^{40}Ar/^{36}Ar ratio (Supplementary Table 7). The log-likelihood function minimized in MCMC sampling is $-\frac{1}{n}\sum_{i=1}^{n}(O_i - E_i)^2/\sigma_i^2$ where n is the number of constraints, O_i are the model outputs, E_i are the constraint values and σ_i their uncertainties. The large uncertainty in the continental crust ^{40}K concentration (Supplementary Table 7) encompasses the range of different estimates[73]. The large uncertainty in the bulk mantle ^{40}Ar/^{36}Ar ratio reflects the range of values measured in MORBs and OIBs[3]. Because Earth's K concentration strongly affects the distribution of terrestrial ^{40}Ar, we do not assume any particular value for K_{BSE} but rather allow it to vary as a free parameter within a wide range encompassing published estimates (Extended Data Fig. 1) so that we can assess values that are required to match the K–Ar observational constraints. We also note that previous models of the K–Ar system[9–12,22,23,26] have not considered the possibility of atmospheric Ar subduction.

Our MCMC implementation uses the affine-invariant sampler[74] coded in the Python package emcee[75]. We sample from uniform prior distributions listed in Table 1. We discard the first 25,000 MCMC samples as burn-in and use the subsequent 25,000 samples as the posterior parameter distributions to ensure that sampling has stabilized and model outputs match the observational constraints (Supplementary Figs. 1–6). The median and middle 95% of the posterior distributions (Table 1) are considered the 'best-fit' parameter values and a measure of their uncertainties. In addition, the distributions are shown as bivariate probability density plots (Supplementary Figs. 7–12), which allows for visualization of correlations with between parameters. These plots detail the physical and chemical scenarios required to match the K–Ar observations, as discussed in the main text.

Ar–He mixing model. We hypothesize that subducted oceanic crust delivering atmospheric Ar to the mantle can explain the distribution of mantle ^{40}Ar/^{36}Ar ratios, including low values seen in OIBs. However, very high ^{4}He/^{3}He ratios in subducted oceanic crust[76] could potentially overprint primordial (low) ^{4}He/^{3}He ratios in OIBs. Here we describe an illustrative mixing model between subducted oceanic crust and primordial material to demonstrate that addition of subducted oceanic crust to primordial material can strongly influence ^{40}Ar/^{36}Ar while preserving primordial ^{4}He/^{3}He. Ar endmember

compositions come from our dlnρ64 model. The primordial component has 1.18×10^{10} atoms g^{-1} ^{36}Ar, and ^{40}Ar/^{36}Ar = 36,800. The subducted oceanic crust component has 4.87×10^{10} atoms g^{-1} ^{36}Ar, and ^{40}Ar/^{36}Ar = 2,100 (averages of 1.0 ± 0.1 Gyr old eclogite tracers). We assume that the primordial component has 6.10×10^{10} atoms g^{-1} ^{3}He (ref. [71]) and ^{4}He/^{3}He = 6,000 and that the subducted oceanic crust component has 2.48×10^{6} atoms g^{-1} ^{3}He (assuming 1 Gyr old crust with 47 ppb U and 99 ppb Th (ref. [77])) and ^{4}He/^{3}He = 10^{8}. Adding 25% subducted oceanic crust to the primordial endmember decreases ^{40}Ar/^{36}Ar from 36,800 to 16,700 but only increases ^{4}He/^{3}He from 6,000 to 7,200. This mixing model is simplistic in that the endmember compositions and mixing proportions are largely hypothetical, the mixture does not consider other components such as depleted MORB mantle and atmosphere-derived Ar and radiogenic He are contained in different parts of the subducting slabs, so they may be physically separated during subduction and mantle convection. Despite these simplifications, the calculation demonstrates that subducted oceanic crust could have high enough ^{36}Ar and low enough ^{3}He concentrations to strongly affect Ar but not He isotopes.

Timescaling in the dlnρ64ts model. Our geodynamic models have constant internal heating and core–mantle boundary and surface temperatures, resulting in nearly constant convective vigour with time[14]. We therefore simulate the effect of early enhanced convective vigour in the dlnρ64 model by modifying the time steps such that the total model time remains 4.55 Gyr but with shorter intervals between early time steps and longer intervals between later ones. To map rescaled time t' to original time t, we chose a hyperbolic function $t' = (k\,t_E\,t + t)/(k\,t + 1)$ where t_E is the age of the Earth (assumed to be 4.55 Gyr) and k is a parameter that controls the extent of rescaling. The maximum scaling we can achieve (with $k = -0.1$ Gyr^{-1}) yields a model, dlnρ64ts, with plate speeds approximately doubled at the model start and decreasing roughly linearly with time (Fig. 3b). The increased Hadean–Archaean mantle processing rate in the dlnρ64ts model is still slower than that required by models of Pu–U–Xe evolution, which can be up to 7–10 times the modern processing rate[53,54]. The maximum rescaling possible by our methodology is limited by a requirement in our geochemical post-processing for a sufficient number of tracers to experience melting during each time step, which is not met when convective speeds become very slow towards the end of the model.

Data availability

No new data were collected as part of this study. All data used in this study are available from the cited references.

Code availability

The geodynamic and geochemical model codes are available from the authors upon request. The code used for MCMC sampling is available from https://github.com/dfm/emcee.

References

56. Jones, R. E. et al. Origins of the terrestrial Hf–Nd mantle array: evidence from a combined geodynamical–geochemical approach. *Earth Planet. Sci. Lett.* **518**, 26–39 (2019).
57. van Keken, P. Cylindrical scaling for dynamical cooling models of the Earth. *Phys. Earth Planet. Inter.* **124**, 119–130 (2001).
58. Gable, C. W., O'Connell, R. J. & Travis, B. J. Convection in three dimensions with surface plates: generation of toroidal flow. *J. Geophys. Res. Solid Earth* **96**, 8391–8405 (1991).
59. Christensen, U. R. & Hofmann, A. W. Segregation of subducted oceanic crust in the convecting mantle. *J. Geophys. Res. Solid Earth* **99**, 19867–19884 (1994).
60. Lithgow-Bertelloni, C. & Richards, M. A. The dynamics of Cenozoic and Mesozoic plate motions. *Rev. Geophys.* **36**, 27–78 (1998).
61. Pollack, H. N., Hurter, S. J. & Johnson, J. R. Heat flow from the Earth's interior: analysis of the global data set. *Rev. Geophys.* **31**, 267–280 (1993).
62. Dasgupta, R. & Hirschmann, M. M. Melting in the Earth's deep upper mantle caused by carbon dioxide. *Nature* **440**, 659–662 (2006).
63. Nakagawa, T. & Tackley, P. J. Influence of initial CMB temperature and other parameters on the thermal evolution of Earth's core resulting from thermochemical spherical mantle convection. *Geochem. Geophys. Geosys.* **11**, Q06001 (2010).
64. Nakagawa, T., Tackley, P. J., Deschamps, F. & Connolly, J. A. D. The influence of MORB and harzburgite composition on thermo-chemical mantle convection in a 3-D spherical shell with self-consistently calculated mineral physics. *Earth Planet. Sci. Lett.* **296**, 403–412 (2010).
65. Brandenburg, J. P. & van Keken, P. E. Deep storage of oceanic crust in a vigorously convecting mantle. *J. Geophys. Res.* **112**, B06403 (2007).
66. Li, M., McNamara, A. K. & Garnero, E. J. Chemical complexity of hotspots caused by cycling oceanic crust through mantle reservoirs. *Nat. Geosci.* **7**, 366–370 (2014).
67. Billen, M. I. Modeling the dynamics of subducting slabs. *Annu. Rev. Earth Planet. Sci.* **36**, 325–356 (2008).
68. Hurley, P. M. & Rand, J. R. Pre-drift continental nuclei. *Science* **164**, 1229–1242 (1969).
69. Porcelli, D., Ballentine, C. J. & Wieler, R. An overview of noble gas geochemistry and cosmochemistry. *Rev. Mineral. Geochem.* **47**, 1–19 (2002).
70. Lee, J. Y. et al. A redetermination of the isotopic abundances of atmospheric Ar. *Geochim. Cosmochim. Acta* **70**, 4507–4512 (2006).
71. Halliday, A. N. The origins of volatiles in the terrestrial planets. *Geochim. Cosmochim. Acta* **105**, 146–171 (2013).
72. Turekian, K. K. The terrestrial economy of helium and argon. *Geochim. Cosmochim. Acta* **17**, 37–43 (1959).
73. Rudnick, R. L. & Gao, S. in *Treatise on Geochemistry* 2nd edn, Vol. 4 (ed. Rudnick, R. L.) 1–51 (Elsevier, 2014).
74. Goodman, J. & Weare, J. Ensemble samplers with affine invariance. *Comm. Appl. Math. Comp. Sci.* **5**, 65–80 (2010).
75. Foreman-Mackey, D., Hogg, D. W., Lang, D. & Goodman, J. emcee: the MCMC hammer. *Publ. Astron. Soc. Pac.* **125**, 306–312 (2013).
76. Kurz, M. D., Jenkins, W. J. & Hart, S. R. Helium isotopic systematics of oceanic islands and mantle heterogeneity. *Nature* **297**, 43–47 (1982).
77. Kelley, K. A., Plank, T., Farr, L., Ludden, J. & Staudigel, H. Subduction cycling of U, Th, and Pb. *Earth Planet. Sci. Lett.* **234**, 369–383 (2005).
78. Allègre, C. J., Poirier, J. P., Humler, E. & Hofmann, A. W. The chemical composition of the Earth. *Earth Planet. Sci. Lett.* **134**, 515–526 (1995).
79. Hart, S. R. & Zindler, A. In search of a bulk-Earth composition. *Chem. Geol.* **57**, 247–267 (1986).
80. Jagoutz, E. et al. The abundances of major, minor and trace elements in the Earth's mantle as derived from primitive ultramafic nodules. In *Proc. 10th Lunar and Planetary Science Conference* 2031–2050 (Pergamon Press, 1979).
81. Lyubetskaya, T. & Korenaga, J. Chemical composition of Earth's primitive mantle and its variance: 1. Methods and results. *J. Geophys. Res. Solid Earth* **112**, B03211 (2007).
82. McDonough, W. F. & Sun, S. S. The composition of the Earth. *Chem. Geol.* **120**, 223–253 (1995).
83. Palme, H. & O'Neill, H. St. C. in *Treatise on Geochemistry* 2nd edn, Vol. 3 (ed. Carlson, R. W.) 1–39 (Elsevier, 2014).
84. Huang, Y., Chubakov, V., Mantovani, F., Rudnick, R. L. & McDonough, W. F. A reference Earth model for the heat-producing elements and associated geoneutrino flux. *Geochem. Geophys. Geosyst.* **14**, 2003–2029 (2013).
85. Plank, T. in *Treatise on Geochemistry* 2nd edn, Vol. 4 (ed. Rudnick, R. L.) 607–629 (Elsevier, 2014).
86. Turner, S. J. & Langmuir, C. H. The global chemical systematics of arc front stratovolcanoes: evaluating the role of crustal processes. *Earth Planet. Sci. Lett.* **422**, 182–193 (2015).

Acknowledgements

J.M.T. and P.E.v.K. acknowledge funding from NSF CSEDI grant 1664642. J.M.T. acknowledges support from a Peter Buck Postdoctoral Fellowship. C.J.B. acknowledges funding from the NERC Deep Mantle Volatiles consortium, NE/M000427/1.

Author contributions

P.E.v.K. developed the geodynamic models; J.M.T. and P.E.v.K. developed the geochemical models with input from C.J.B.; all authors analysed the results; J.M.T. wrote the manuscript with input from P.E.v.K. and C.J.B.

Competing interests

The authors declare no competing interests.

Additional information

Extended data is available for this paper at https://doi.org/10.1038/s41561-021-00870-6.

Supplementary information The online version contains supplementary material available at https://doi.org/10.1038/s41561-021-00870-6.

Correspondence and requests for materials should be addressed to Jonathan M. Tucker.

Peer review information *Nature Geoscience* thanks Philippe Sarda and the other, anonymous, reviewer(s) for their contribution to the peer review of this work. Primary Handling Editor: Rebecca Neely.

Reprints and permissions information is available at www.nature.com/reprints.

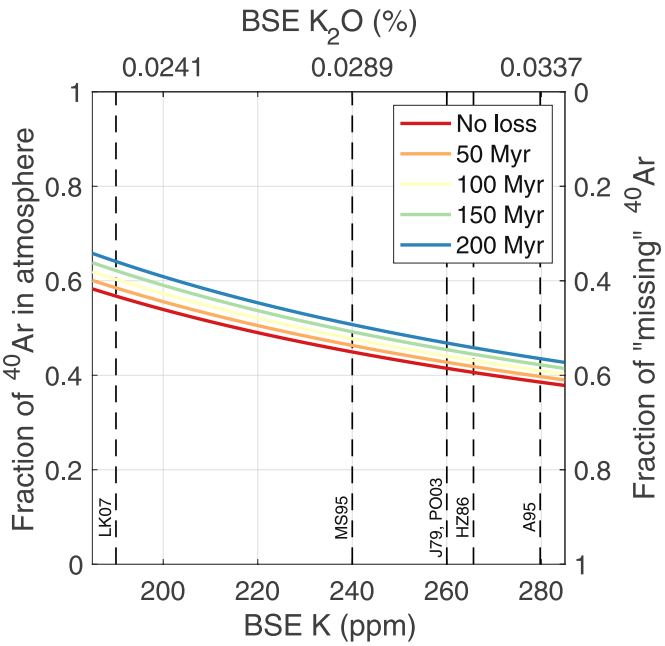

Extended Data Fig. 1 | Fraction of terrestrial ^{40}Ar in the atmosphere for different BSE K concentrations (red line). The other colored lines assume that all ^{40}Ar produced before the specified time is lost to space, for example by impacts. Due to the long half-life of ^{40}K, the amount of ^{40}Ar produced and lost even after 200 Ma hardly affects the terrestrial ^{40}Ar budget and the missing Ar paradox. Furthermore, these calculations assume efficient degassing such that all ^{40}Ar produced within the specified time is subject to atmospheric loss. Any ^{40}Ar retained within the Earth would reduce the effect. A95 = Allègre et al.[78]; HZ86 = Hart and Zindler[79]; J79 = Jagoutz et al.[80] LK07 = Lyubetskaya and Korenaga[81]; MS95 = McDonough and Sun[82]; PO03 = Palme and O'Neill[83].

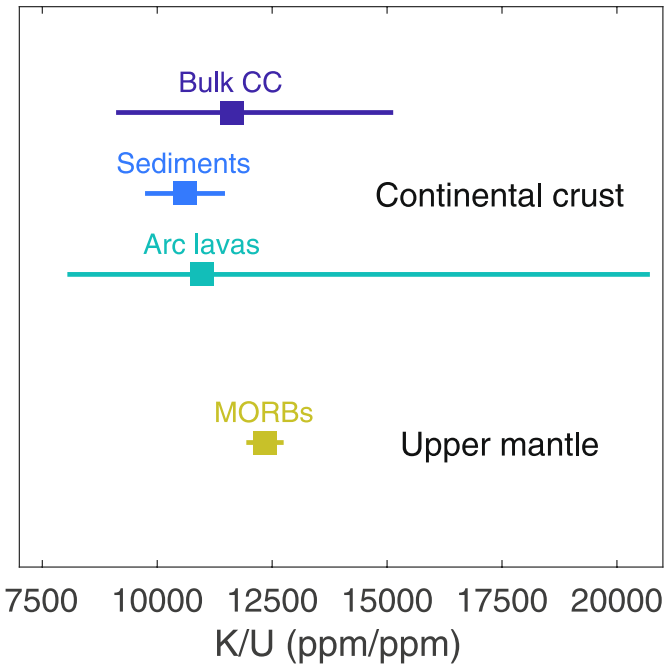

Extended Data Fig. 2 | K/U ratios in the upper mantle and continental crust. Bulk continental crust is 11600_{-2500}^{+3500} ref. [84]); sediments are 10600 ± 900 (2.21 ± 0.14\$% K_2O, 1.73 ± 0.09 ppm U; ref. [85]); arc lavas are 11000_{-2900}^{+9700} based on the median and $1-\sigma$ range of arc segment averages[86]; MORB is 12300 ± 400 (ref. [32]). The similarity between K/U ratios of the upper mantle and continental crust suggest that K/U fractionation during subduction does not substantially alter the global K and U budgets, and that MORBs provide a reasonable estimate for the BSE.